



HAL
open science

Experimental and numerical analysis of dielectric polarization effects in near-surface earth materials in the 100 Hz–10 MHz frequency range: First interpretation paths

A Tabbagh, B Souffaché, D Jougnot, A Mainault, F Rejiba, P M Adler, C Schamper, J Thiesson, C Finco, A Mendieta, et al.

► To cite this version:

A Tabbagh, B Souffaché, D Jougnot, A Mainault, F Rejiba, et al.. Experimental and numerical analysis of dielectric polarization effects in near-surface earth materials in the 100 Hz–10 MHz frequency range: First interpretation paths. *Near Surface Geophysics*, 2024, 10.1002/nsg.12302 . insu-04591946

HAL Id: insu-04591946

<https://insu.hal.science/insu-04591946v1>

Submitted on 29 May 2024












HAL is a multi-disciplinary open access archive for the deposit and dissemination of scientific research documents, whether they are published or not. The documents may come from teaching and research institutions in France or abroad, or from public or private research centers.

L'archive ouverte pluridisciplinaire **HAL**, est destinée au dépôt et à la diffusion de documents scientifiques de niveau recherche, publiés ou non, émanant des établissements d'enseignement et de recherche français ou étrangers, des laboratoires publics ou privés.



Distributed under a Creative Commons Attribution - NonCommercial - NoDerivatives 4.0 International License

Experimental and numerical analysis of dielectric polarization effects in near-surface earth materials in the 100 Hz–10 MHz frequency range: First interpretation paths

A. Tabbagh¹  | B. Souffaché¹  | D. Jougnot¹  | A. Mainault¹  | F. Rejiba¹  |
P. M. Adler¹ | C. Schamper¹  | J. Thiesson¹  | C. Finco²  | A. Mendieta³  |
F. Rembert⁴  | R. Guérin¹  | C. Camerlynck¹

¹Sorbonne Université, CNRS, EPHE, UMR 7619 Métis, Paris, France

²Cerema, ENDSUM, le grand Quevilly, France

³Institut de Physique du Globe de Paris, université Paris-Cité, CNRS, Paris, France

⁴Université Orléans, CNRS, BRGM, OSUC, ISTO, UMR 7327, Orléans, France

Correspondence

A. Tabbagh, Sorbonne Université, CNRS, EPHE, UMR 7619 Métis, 4 Place Jussieu 75252, Paris Cedex 05, France.
Email: alain.tabbagh@upmc.fr

Summary

The recent developments of electromagnetic induction and electrostatic prospecting devices dedicated to critical zone surveys in both rural and urban contexts necessitate improving the interpretation of electrical properties through complementary laboratory studies. In a first interpretation step, the various experimental results obtained in the 100 Hz–10 MHz frequency range can be empirically fitted by a simple six-term formula. It allows the reproduction of the logarithmic decrease of the real component of the effective relative permittivity and its corresponding imaginary component, the part associated with the direct current conductivity, one Cole–Cole relaxation and the real and imaginary components of the high-frequency relative permittivity. For elucidating physical phenomena contributing to both the logarithmic decrease and the observed Cole–Cole relaxation, we first consider the Maxwell–Wagner–Sillars polarization. Using the method of moments, we establish that this continuous medium approach can reproduce a large range of relaxation characteristics. At the microscopic scale, the possible role of the rotation of the water molecules bound to solid grains is then investigated. In this case, contrary to the Maxwell–Wagner–Sillars approach, the relaxation parameters do not depend on the external medium properties.

KEYWORDS

dielectric properties, electromagnetism, hydrogeophysics, modelling

INTRODUCTION

A better characterization of the so-called critical zone, from natural soils to urban artificial structures, is of paramount importance for the management of the natural and cultural environments (Capello et al., 2021). Consequently, the application of geophysical methods to the near-surface underwent large developments in the last decades; rapid measurements of the physical

properties allowing dense data sampling over extended surfaces have been achieved. The various methods measuring the electrical resistivity played a major role (Hermans et al., 2023; Pellerin, 2002; Samouëlian et al., 2005; Viscarra-Rossel & Adamchuk, 2013), but significant progress is still conceivable in the electrical/electromagnetic domain.

Besides the direct current (DC) resistivity method (Gebbers et al., 2009), the use of electromagnetic

This is an open access article under the terms of the [Creative Commons Attribution-NonCommercial-NoDerivs](https://creativecommons.org/licenses/by-nc-nd/4.0/) License, which permits use and distribution in any medium, provided the original work is properly cited, the use is non-commercial and no modifications or adaptations are made.

© 2024 The Authors. *Near Surface Geophysics* published by John Wiley & Sons Ltd on behalf of European Association of Geoscientists and Engineers.

induction (EMI) instruments (Corwin & Lesch, 2003) has been and is largely used in open areas, whereas, in urban contexts, the electrostatic method, also called capacitively coupled resistivity (Kuras et al., 2006; Tabbagh et al., 1993), allows us to overcome both the impact of metallic disturbers and the absorption of ground penetrating radar (GPR) signals by clayey materials. Due to technical limitations, most of the corresponding devices use low frequencies in the 10–100 kHz range, but several attempts reached the 300 kHz–3 MHz medium frequency band, with both frequency (Glaser et al., 2022; Kessouri et al., 2016) and time-domain (Auken et al., 2019; Wright et al., 2000) instruments. In these frequency ranges, between frequencies dominated by conductivity and those by dielectric permittivity, electrical polarization cannot be neglected in comparison with conductivity (Glaser et al., 2023; Loewer et al., 2017; Tabbagh et al., 2021), and it is necessary to consider the dielectric permittivity together with the electrical conductivity and the magnetic susceptibility. Some interpretations of field results acquired with EMI (e.g., Simon et al., 2019) and electrostatic instruments (e.g., Schamper et al., 2021; Souffaché et al., 2016) led to apparent relative permittivity in accordance with the published laboratory measurements. However, the information that can be extracted from permittivity deserves to be more clearly delineated, which necessitates multiplying both in situ experiments and laboratory studies with undisturbed and synthetic samples in the same frequency range as in surveys. Nevertheless, in order to better assess the role of frequency, our laboratory results have been extended out of the limits of frequency range used in-field to the larger interval (100 Hz–10 MHz).

In physical and chemical domains, the study of the electrical properties versus frequency is generally called dielectric spectroscopy. It is an important branch of chemical analysis and it covers a very large variety of applications (Woodward 2021). In applied geophysics, for both infield and laboratory studies, works and publications were focused on two different frequency domains which can be roughly defined as below 1 kHz and above 20 MHz. At the lowest frequency range (<1 kHz), it is called spectral induced polarization (SIP) (Kemna et al., 2012), the terms ‘complex conductivity measurements’ being also used (Bröner, 2009). For complex multi-phase media such as soils (Kessouri et al., 2019) and rocks, several polarization mechanisms have been proposed to interpret the data when a time-varying electric field is applied (Bücker et al., 2019; Niu et al., 2020). At the highest frequency range (>20 MHz), GPR and time-domain reflectometry are used. There the dominant mechanism is the rotation of the free water molecules which corresponds to permittivity value of 80. This value, about 20 times higher than that of solid grains, determines the effective permittivity. A lack of experimental data and theoretical approaches still

remains between these two frequency domains (Loewer et al., 2017).

Above freezing temperature and in the 100 Hz–10 MHz frequency range, two dominant processes can be called on. The first corresponds to a motion of ions resulting in a non-coincidence between the anion barycentre and the cation barycentre, and the second to the rotation of polar molecules (in practice water molecules). In the first, both anions and cations may move in pore water and be blocked by interfaces. This heterogeneity effect is called interfacial or spatial polarization and is usually classified as Maxwell–Wagner–Sillars polarization when a continuous medium description is used. It may also happen that the cation cloud surrounding the negatively charged solid surfaces is slightly shifted, which is called electrical double layer (EDL) or Stern layer polarization (Binley & Slater, 2020; Kemna et al., 2012; Leroy & Revil, 2009). This EDL may itself play a role in the membrane polarization mechanism where the cation and anion diffusions through pore-throats differ (Bücker & Hördt, 2013). In the second process, the free water (i.e., capillary and gravity water) has a relaxation frequency between 17 GHz and 19 GHz, far above the frequency range considered. However, the relaxation frequencies of the bound water coating the solid surfaces can be around 1 MHz or below, between those of free water and ice.

The present paper is not aimed to be a complete study of the behaviour of the complex permittivity of near-surface geo-materials but, first, to redraw a global picture of experimental laboratory results and of the corresponding empirical model formulation and, second, through numerical modelling of two polarization mechanisms, to progress in the assessment of identification criteria.

CAPACITIVE MEASUREMENTS AND SAMPLES

Choice of the characteristics of the capacitive cell

In the 100 Hz–10 MHz frequency range, for more than 80-years, disc (or slab)-shaped samples have been used. Generally, their diameter is smaller or equal to 10 cm, and their thickness is around 1/10th of the diameter. These discs are inserted into parallel plate capacitive cells. In order to take into account the heterogeneity of the near-surface earth materials, and to work with representative elementary volumes, larger samples of 160 × 160 × 19 mm³ size were chosen. Two metallic plates of the capacitor with larger surfaces of 200 × 200 mm² maintain a uniform electric field on them. In comparison with measurements achieved using four non polarizable electrodes, capacitive cells

(named two electrodes technique in the literature) may generate electrode polarization which corresponds to the blocking of moving ionic charges at the electrode surfaces. This difficulty has been raised up since earlier experiments, and Smith-Rose (1933) explained the increase of the real part of the relative permittivity with the frequency decrease by this sole phenomenon. This interpretation has been reconsidered and Keller and Licastrò (1959) stated that the electrode polarization is 'unimportant' above 50 Hz. Comparisons have also been made between two- and four-electrode techniques (Garrouch & Sharma, 1994; Lesmes & Fry, 2001; Scott et al., 1967); the conclusions were that both techniques fairly agree above 100 Hz and that the electrode polarization is reduced when the plate separation is increased (Ishai et al., 2013). However, two aspects of the instrument used deserve to be detailed.

For such instruments, the relative permittivity is defined by reference to the air response. However to check the sensitivity, it is relevant to analyse the results obtained for a material of low permittivity, a low signal, and to determine the signal over noise ratio (SNR) over the whole frequency range. The noises can originate both from the instrument itself and from the electromagnetic environment and are evidenced by repeating the measurements and observing the dispersion of the results. One first chooses paraffin (relative permittivity value of 2) and expresses the SNR by the ratio between the standard deviation and the median value of the real relative permittivity for each frequency. The evolution of this ratio is illustrated in Figure 1a. It is clear that for low permittivity values (lower than any soil or rock material), the frequency must be higher than 3 kHz in order to get an SNR lower than 1%. Moreover, a material of higher permittivity was used, namely a conductive foam (REF 4454.W, SDEP ACE SA, France) with a relative permittivity of 100 in the middle of the frequency range; the variation of the SNR remains below 1% for all the frequency range (Figure 1a). As the permittivity of the foam corresponds to the lower range of the permittivity of the considered geo-materials, the instrument sensitivity is adequate.

The undesirable electrode polarization effect is commonly checked (Gregory & Clarke, 2005) by comparing the results obtained for samples of various thicknesses corresponding to various distances between the two plates of the capacitive cell. As the sample thickness decreases, the relative weight of the electrode polarization by reference to the bulk polarization of the material increases and the slope of the frequency dependence should be modified. Figure 1b shows the real part of the relative permittivity for $160 \times 160 \text{ mm}^2$ slab samples with three different thicknesses 7, 12 and 19 mm for a sample with 5% of illite and 95% of carbonate powder. One observes a clearly different slope for the 7-mm curve below 300 Hz, whereas the two other thicknesses slopes are consistent.

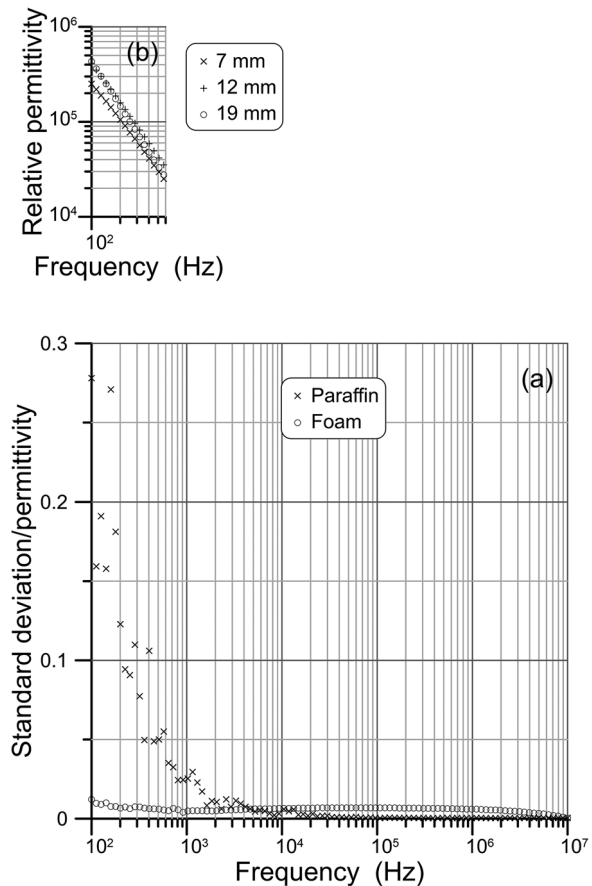


FIGURE 1 Capacitive cell characteristics: (a) ratio of the standard deviation to the median value for a series of measurements on a paraffin sample ($\epsilon' \sim 2$) and a conductive foam ($\epsilon' \sim 100$), (b) frequency variations of the real relative permittivity for various thicknesses of a carbonate/illite slab sample of section $160 \times 160 \text{ mm}^2$.

Measuring instrument

Due to the characteristics of the cell, the signal applied between the two metallic plates generates a uniform electric field. The phase sensitive response is processed by a PSM 1735 vector multi-meter (Phase Sensitive Meter, NumetricQ Ltd.). Frequencies were swept from 100 Hz to 10 MHz.

Samples

The complex permittivity of heterogeneous materials is linked to grain size, shape and orientation relatively to the externally applied electric field, as well as porosity, water saturation and the presence of organic matter (living and dead). In order to interpret complex permittivity data, laboratory studies are here carried out on volumes of about 500 cm^3 . Stiff materials were cut at the cell dimensions in square slab-shaped samples of $16 \times 16 \times 1.9 \text{ cm}^3$, whereas loose materials were simply

packed by hand in the sample holder. All measurements were done at room temperature circa 20°C.

When studying the role of the water content, all samples, whatever their nature, are first saturated by immersion in tap water of conductivity equal to 0.05 S m⁻¹. Effective permittivity measurements were made during free drying; water content was measured by weighing the cell. Each data acquisition was separated from the previous one by a weight loss of approximately 5 g; the last acquisition at the lowest water content was made after drying the sample in an oven at 50°C for 24 h.

GENERAL BEHAVIOUR OF COMPLEX PERMITTIVITY IN UNSATURATED SURFICIAL EARTH MATERIALS IN THE (100 Hz–10 MHz) RANGE

The behaviour of the electrical properties in the considered frequency range is expressed by the complex relative permittivity, $\epsilon_r^* = \epsilon' - i\epsilon''$, with $i = \sqrt{-1}$. The real (or in-phase) part ϵ' corresponds to the electrical polarization and the imaginary (or quadrature) part comprises both the dielectric losses, ϵ'' , and the effect of the DC conductivity $\epsilon'' = \frac{\sigma}{\omega\epsilon_0} + \epsilon''_l$, where ω is the angular frequency, ϵ_0 the vacuum permittivity, and σ the DC conductivity.

Measurements were performed on a wide series of samples for various mineral compounds, water contents and frequencies (dispersion analysis). They agree with previous publications made on rocks samples (Howell & Licastro, 1961) and underline the role of the water content.

The main general observations on all our results are as follows:

1. At a given frequency, for example at 30 kHz in Figure 2, especially when reaching full saturation, both the conductivity and real permittivity are dependent on water content, but the conductivity is more so.
2. For dried materials, the real part of the permittivity is about 3 and thus corresponds to the value adopted by the high-frequency formula (Topp et al., 1980) without observable changes with frequency. The imaginary part is very low and non-measurable.
3. For high water content and/or for conductive materials such as clays, the real part exhibits a regular logarithmic decrease until the high-frequency-independent limit. The imaginary part follows the ω^{-1} decrease associated with the DC conductivity. This is illustrated in Figure 3 for a synthetic carbonate powder sample and for the Fontainebleau sand.
4. At lower water content, that is for unsaturated materials, the real and the imaginary parts exhibit a marked relaxation between the regular logarithmic

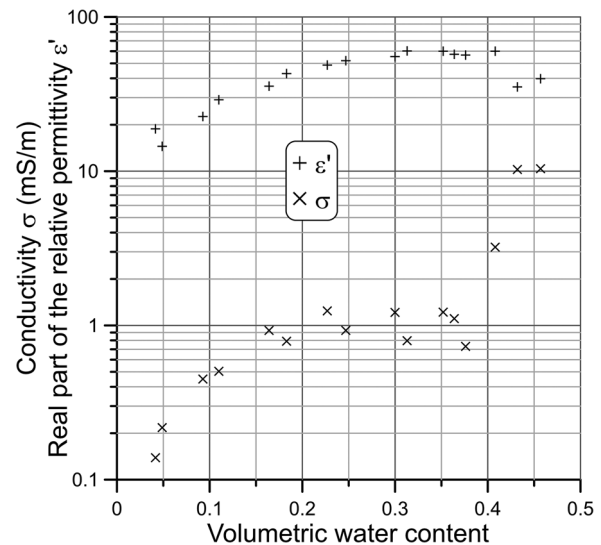


FIGURE 2 Variations of the electrical conductivity and of the real part of the relative permittivity with the volumetric water content θ at 30 kHz, for a sand with a porosity of 0.457. The granularity of this silica sand (Sibelco) corresponds to a uniform distribution between 300 and 600 μm .

decrease and the high-frequency-independent limit (see Figure 4).

PHENOMENOLOGICAL MODELLING OF THE COMPLEX PERMITTIVITY

In the considered frequency range, relaxation is the physical mechanism called on to explain the dispersion, that is the frequency variation, of the complex effective permittivity. To a step change of the applied electric field, that is to an Heaviside function $E_0 Y(t)$, the reaction of a material is delayed and the polarization that

follows $P(t) = P_0(1 - e^{-t/\tau})$ is characterized by the time constant τ related to the activation energy. In the frequency domain, the corresponding Debye's formula is $\frac{P_0}{1+i\omega\tau}$. To mimic a log-normal distribution of the time constants, Cole and Cole (1941) introduced the formula $\frac{P_0}{1+(i\omega\tau)^c}$. Such a relaxation is observed in Figure 4 for partially saturated samples and not in Figure 3 at high water or clay contents.

When there is a series of relaxations whose time constant distribution is large and quasi-uniform, an integration over the time constant leads to a regular logarithmic decrease with frequency for the real part (Figure 3) which can be described by $\epsilon'_j(\frac{\omega}{\omega_j})^{-n}$, and to

an imaginary part $\frac{\pi}{2} \frac{\partial(\epsilon'_j(\frac{\omega}{\omega_j})^{-n})}{\partial \ln(\omega)}$ which is in fact quasi-independent on frequency. This general behaviour is well established in dielectric spectroscopy (Woodward, 2021) as in magnetism (Mullins & Tite, 1973). Conse-

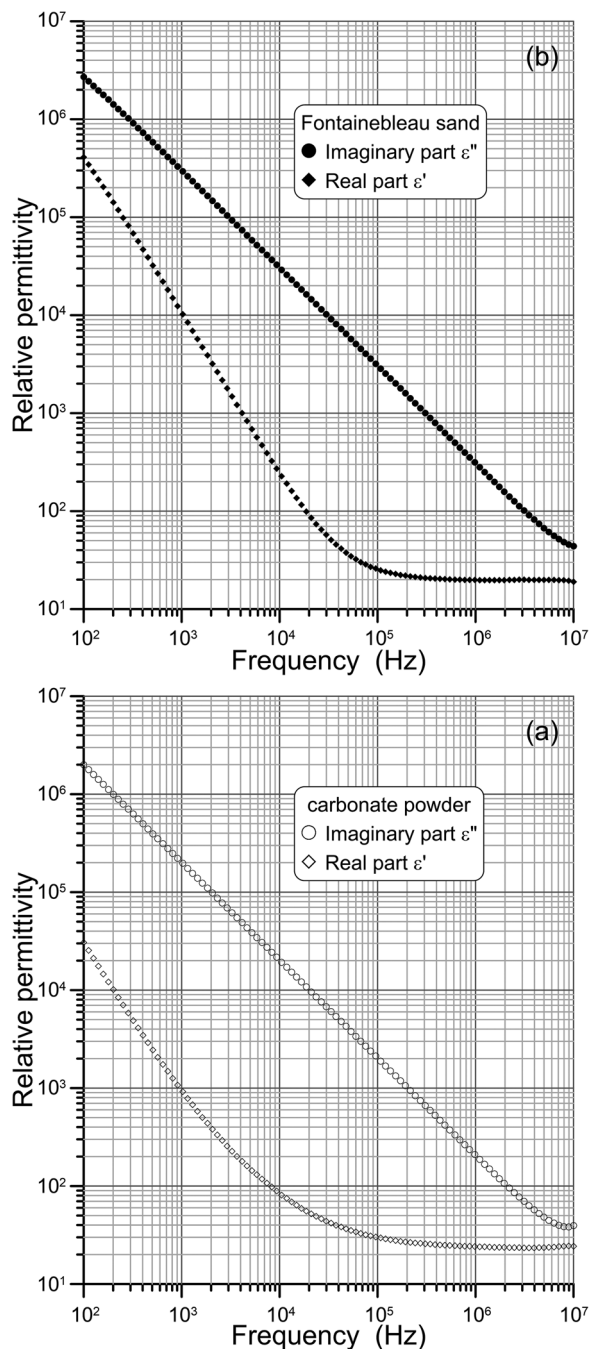


FIGURE 3 Frequency variation of the effective relative permittivity at high water content (with $\sigma_w = 0.05 \text{ S m}^{-1}$): (a) carbonate powder saturated at $\theta = 0.415$, for which the interpretation parameters are $n = 1.48$, $\epsilon'_j = 30,700$, $\sigma = 11.3 \text{ mS m}^{-1}$, $\epsilon'_{\text{HF}} = 25$, $\epsilon''_{\text{HF}} = 3.3$. The size distribution is centred around $30 \mu\text{m}$; (b) Fontainebleau sand saturated at $\theta = 0.395$, for which the interpretation parameters are $n = 1.64$, $\epsilon_j = 409,050$, $\sigma = 16.6 \text{ mS m}^{-1}$, $\epsilon'_{\text{HF}} = 21$, $\epsilon''_{\text{HF}} = 7.0$. This pure silica sand has a very narrow size distribution centred at $200 \mu\text{m}$.

quently, Jonscher (1977) presented this behaviour as universal. However, in moist soils and rocks, the DC conductivity contribution to the imaginary part $\frac{\sigma}{\omega\epsilon_0}$ overrides the other mechanisms.

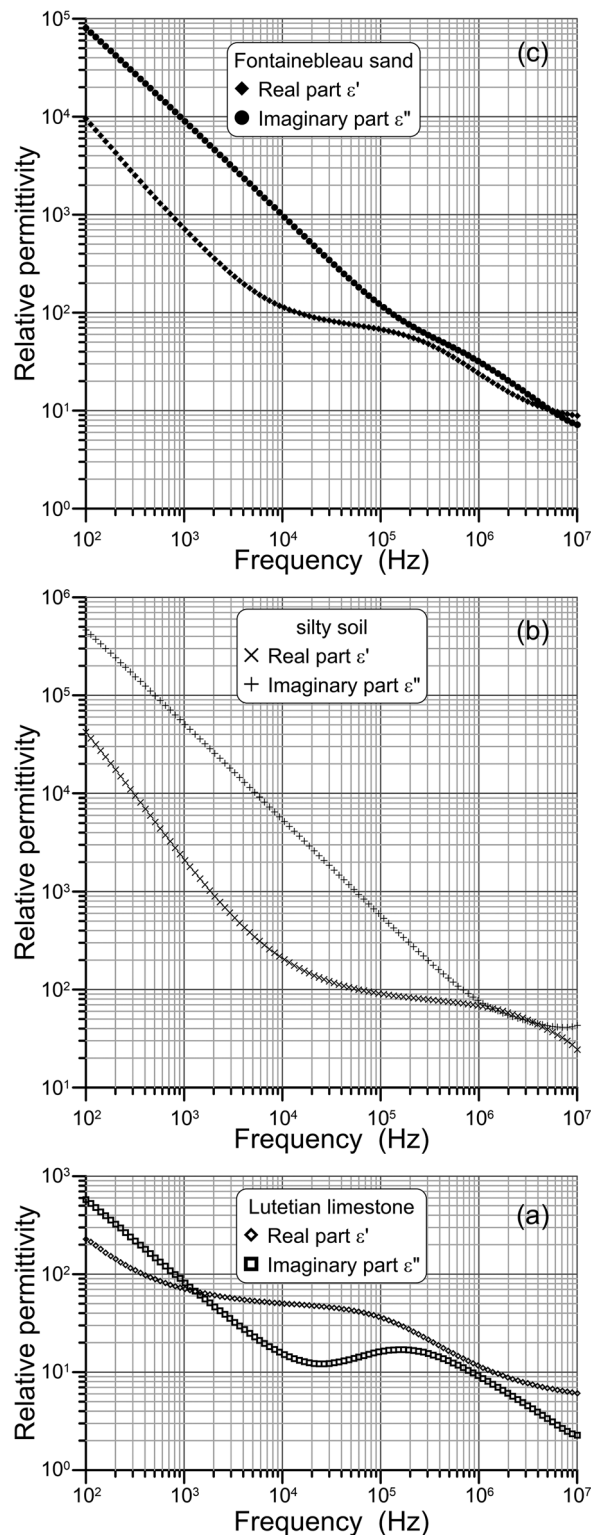


FIGURE 4 Frequency variations of the effective complex relative permittivity, unsaturated samples: (a) Lutetian limestone of $\theta = 0.132$; the interpretation parameters are $n = 0.88$, $\epsilon'_j = 560$, $\sigma = 0.0125 \text{ mS m}^{-1}$, $\epsilon'_{\text{HF}} = 9.0$, $\epsilon''_{\text{HF}} = 1.7$, $\tau = 0.333 \mu\text{s}$, $c = 0.89$, $\Delta\epsilon_p = 32$; (b) silty soil of $\theta = 0.206$; the interpretation parameters are $n = 1.28$, $\epsilon'_j = 42,050$, $\sigma = 3.0 \text{ mS m}^{-1}$, $\epsilon'_{\text{HF}} = 20$, $\epsilon''_{\text{HF}} = 5.0$, $\tau = 0.13 \mu\text{s}$, $c = 0.65$, $\Delta\epsilon_p = 77$; (c) Fontainebleau sand of $\theta = 0.153$; the interpretation parameters are $n = 1.12$, $\epsilon'_j = 9500$, $\sigma = 0.54 \text{ mS m}^{-1}$, $\epsilon'_{\text{HF}} = 10$, $\epsilon''_{\text{HF}} = 2.2$, $\tau = 0.23 \mu\text{s}$, $c = 0.94$, $\Delta\epsilon_p = 45$.

In order to fit the previous general observations presented before, six terms are included in the complex permittivity $\varepsilon_r^*(\omega)$:

$$\varepsilon_r^*(\omega) = \varepsilon_j' \left(\frac{\omega}{\omega_j} \right)^{-n} - i \frac{\pi}{2} \frac{\partial \left(\varepsilon_j' \left(\frac{\omega}{\omega_j} \right)^{-n} \right)}{\partial \ln(\omega)} - i \frac{\sigma}{\omega \varepsilon_0} + \frac{\Delta \varepsilon_p}{1 + (i\omega\tau)^c} + \varepsilon_{HF}' - i \varepsilon_{HF}'' \quad (1)$$

First the 'Jonscher type' logarithmic decrease of the real part is characterized by the negative exponent n and the starting value ε_j' at 100 Hz (the corresponding angular frequency ω_j is used in the equation); to this term is added the corresponding imaginary part. The third term reflects the effect on the imaginary part of the DC conductivity and the fourth one the effect of the Cole–Cole type relaxation. This Cole–Cole empirical expression (Cole & Cole, 1941) comprises the relative permittivity strength $\Delta \varepsilon_p$, the central time constant τ , and the exponent c which characterizes the relaxation distribution around τ . Those Cole–Cole parameters are particularly useful when dealing with partially saturated media as in Figure 5. Finally, the real and imaginary parts of the high frequency permittivity are given by the fifth and sixth terms and are necessary to fit the asymptotic values at frequencies above several MHz (Figures 3–5).

The Jonscher variation has been observed for sedimentary rocks (Knight & Nur, 1987) and the usefulness of the second term can be illustrated in Figure 5 for a low conductivity sample, with a better fit of the imaginary part when the second term is considered (Figure 5b) compared to the fit without it (Figure 5a). In accordance with the stability (Topp et al., 1980) of the high frequency dielectric permittivity up to several GHz, the two last terms are independent of frequency. Globally (Equation 1) is useful for fitting data, but it does not relate the permittivity values to the intrinsic physical and chemical properties of the samples at microscopic scales.

INTERPRETATIVE PHYSICAL PHENOMENA

The interpretation cannot be limited to a global phenomenological description of sample behaviours with a limited number of parameters but has to attempt linking the observations (and the interpreted parameters) to intrinsic characteristics of the considered material such as the pore and throat sizes, permeability and fluid storage capacity whose knowledge allows the assessment of water resources and more generally of underground petro-physical properties. For example, GPR measurements not only allow the location of underground reflectors, but can also give values of the

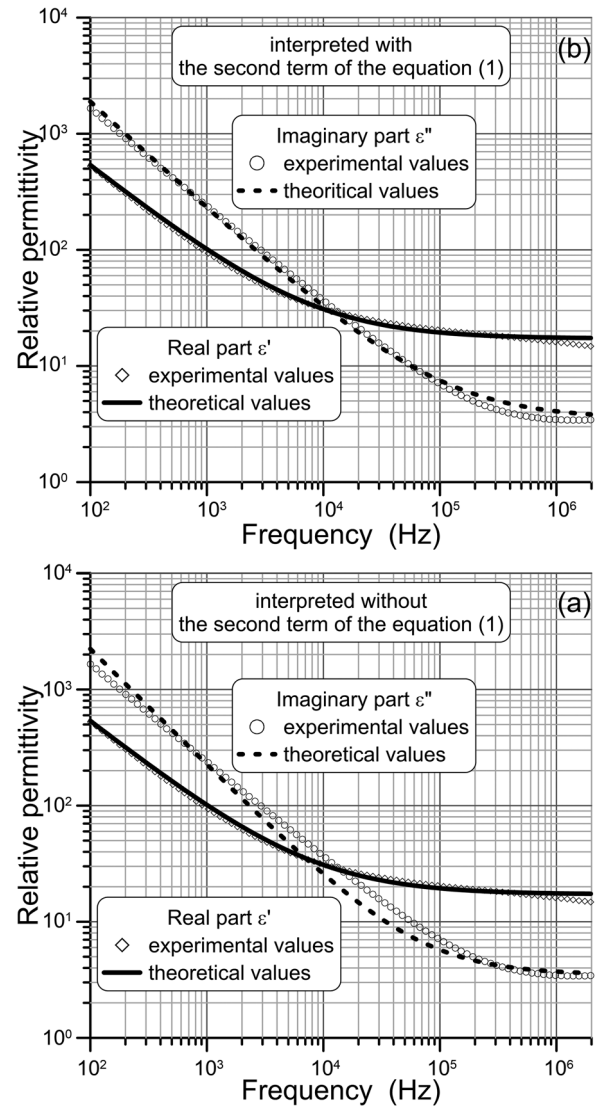


FIGURE 5 Frequency variations of the effective complex relative permittivity for a carbonate powder synthetic sample containing 30% of smectite, with $\theta = 0.0535$; the interpretation parameters are $n = 0.79$, $\varepsilon_j' = 520$, $\sigma = 6.9 \mu\text{S m}^{-1}$, $\varepsilon_{HF}' = 17.2$, $\varepsilon_{HF}'' = 3.5$. (a) Interpreted without the second term of Equation (1), rms global error 0.13; (b) interpreted with the second term of Equation (1), rms global error reduced to 0.0675.

volumetric water content of the various soil volumes. In the SIP domain, several attempts have been achieved to determine the hydraulic permeability (Koch et al., 2011; Nordsiek et al., 2016; Revil et al., 2015; Robinson et al., 2018; Slater & Glaser, 2003); namely Glaser (2021) demonstrated the effectiveness of hydraulic conductivity prediction models using physical and electrical parameters at a single site. To evidence, biofilms (Albrecht et al., 2011; Ntarlagiannis & Ferguson, 2009) have also been tested and so on. These approaches can be extended to the considered frequency range. However, most of the literature qualify the electrical polarization behaviour observed in the 100 Hz–10 MHz frequency range as 'Maxwell–Wagner–Sillars' polarization (Loewer

et al., 2017; Revil, 2013). Such a name corresponds to a continuous medium description using two electrical properties, the conductivity and the permittivity, without any information about the microscopic structure of the considered material. It is thus necessary, in a first step, to delineate the characteristics specific to the Maxwell–Wagner–Sillars polarization and in the following steps to consider different possible models of the microscopic structure and behaviour. As a start of this second step, the present study considers a ‘bound water molecules’ model.

Modelling by Maxwell–Wagner–Sillars polarization

This polarization results from a contrast between two media with different conductivities and permittivities. In this approach, the media are considered continuous, and no hypothesis is proposed about the underlying microscopic physical phenomena. Consequently, several phenomena can fit with the ‘Maxwell–Wagner–Sillars’ polarization, and this denomination can play the role of ‘hold all’. The proper characteristics of this approach in terms of amplitude and time constant should nevertheless be better grasped. This model has been followed and discussed by numerous authors with more or less details (Alvarez, 1973; de Lima & Sharma, 1992), but it is important to start here by recalling the simplest case of the sphere in a uniform surrounding medium.

Maxwell–Wagner polarization: unique spherical contrasting volume

A uniform primary electric field, \vec{E}_0 , is applied on a spherical volume of radius a , conductivity σ_1 and relative permittivity ϵ_1 . It is located in an infinite medium of conductivity σ_2 and permittivity ϵ_2 . These four properties are time independent. In the static approximation where the equation $\nabla(\epsilon_r^* \nabla V) = 0$ is solved, the sphere is equivalent to a dipole of moment, $\vec{M} = 4\pi a^3 \vec{E}_0 \frac{\epsilon_1^* - \epsilon_2^*}{\epsilon_1^* + 2\epsilon_2^*}$, where the properties are expressed by the complex permittivities:

$$\epsilon_1^* = \epsilon_1 + \frac{\sigma_1}{i\omega\epsilon_0} \quad (2)$$

and

$$\epsilon_2^* = \epsilon_2 + \frac{\sigma_2}{i\omega\epsilon_0}. \quad (3)$$

At one point outside the sphere, one calculates the secondary electric field generated by the sphere. The frequency variations of this field do not depend on a , but only on $\frac{\epsilon_1^* - \epsilon_2^*}{\epsilon_1^* + 2\epsilon_2^*}$. The shape (spherical) governs this

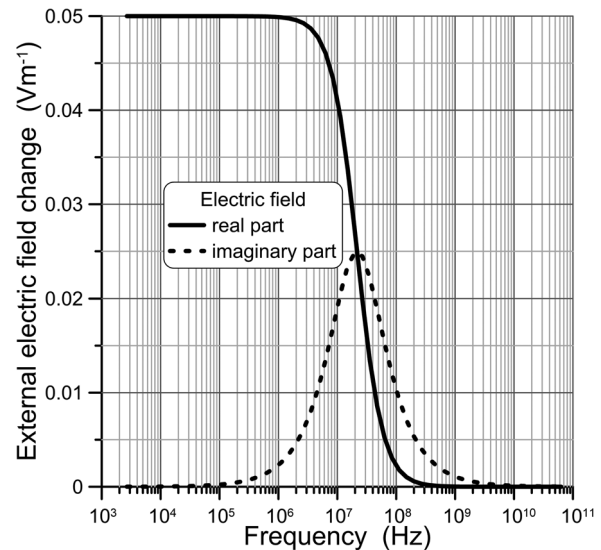


FIGURE 6 Frequency variations of the electric field generated by a spherical volume when $\sigma_1 = 100 \text{ mS m}^{-1}$, $\epsilon_1 = 80$, $\sigma_2 = 10 \text{ mS m}^{-1}$ and $\epsilon_2 = 10$. The resulting time constant is $\tau = 7.16 \text{ ns}$.

TABLE 1 Relaxation parameters as functions of conductivities for the Maxwell–Wagner–Sillars polarization of a unique spherical body of $\epsilon_2 = 80$ in a surrounding medium of $\epsilon_1 = 10$.

σ_1 $\sigma_2 \text{ (mS m}^{-1}\text{)}$	100	31.6	10	3.16
(a) Time constants (ns)				
100	2.90	3.75	4.08	4.19
31.6	5.29	9.19	11.84	12.90
10	7.16	16.73	29.05	37.5
3.16	7.98	22.66	52.9	91.9
1	8.37	25.25	71.6	167.3
(b) $\Delta\epsilon_p$				
100	0.700	0.995	1.13	1.18
3.16	0.281	0.700	0.995	1.13
10	0.050	0.281	0.700	0.995
3.16	0.211	0.050	0.281	0.700
1	0.271	0.211	0.05	0.281

result, but the geometric scale has no influence. The resulting field variations are presented in Figure 6 where its real and imaginary parts are seen to exactly correspond to the Debye formula with the peak amplitude of the imaginary part being half of the real part strength.

In Table 1a,b, the effect of the property contrasts is illustrated by the conductivity dependence of both the time constants τ and the strength amplitude $\Delta\epsilon_p$, which are deduced after fitting the Debye formula (the permittivity values remain at $\epsilon_1 = 80$ and $\epsilon_2 = 10$). τ increases when the conductivities σ_1 and σ_2 decrease; when both are divided by 10, τ is multiplied by 10. The strength amplitudes $\Delta\epsilon_p$ vary and are governed by conductivity ratios (the same $\Delta\epsilon_p$ values along diagonals in Table 1b).

In fact, a contrasting cell acts as an electrically polarized volume; however, such cells, which may be numerous, are inevitably coupled together and can have different electrical properties. Note also that, if a sphere can be relevant to describe water drops, it is not adequate for the platelet shaped particles found in clays. Thus, the number of possible simulations is very large and hereafter one will consider three cases, namely coupled identical isotropic cells (spheres/cubes) with random locations, coupled and non-identical isotropic cells and, finally, a non-isotropic platelet.

Effective complex permittivity of a volume comprising a set of elementary isotropic identical cells coupled together

Here, the method of moments, MoM (Tabbagh et al., 2002), is used to calculate the effective relative permittivity corresponding to a random distribution of polarized cells inside a volume of conductivity σ_2 and relative permittivity ε_2 . On this volume is applied a uniform primary electric field; the size of the volume is considered sufficiently small for the static approximation to be used. In the volume are randomly located a series of cubic or spherical isotropic cells of conductivity σ_1 and relative permittivity ε_1 . The cells are coupled together and the resulting effective relative permittivity of the volume is deduced from the total field outside the volume. In the MoM, one can easily change the content of the polarizable cells and/or their properties. By adopting the same properties as in Figure 6, $\sigma_1 = 100 \text{ mS m}^{-1}$, $\varepsilon_1 = 80$, $\sigma_2 = 10 \text{ mS m}^{-1}$ and $\varepsilon_2 = 10$, one obtains the same frequency variations. The effect of the cell content is illustrated in Table 2a–c where the variations of the effective conductivity and of the amplitude of the strength are increasing as expected, both are multiplied by around 2 when the volumetric content is multiplied by 4, but where the increase of the time constant is very small. The comparison among Table 2a–c underlines the effect of the cell permittivity on the time constant. When both σ_1 and σ_2 are divided by 10, the results, displayed in Table 3, verify and confirm two important facts: Although the effective conductivity is divided by 10, the amplitude of the strength is unchanged (the ratio σ_1/σ_2 remains identical in Tables 2b and 3), and the time constants are multiplied by 10.

Effective complex permittivity of an isotropic volume comprising a set of elementary isotropic, but of differing properties coupled cells

In this section, the conductivity and/or the permittivity are different from one cell to another, but the cell volumes remain identical. The possible simulations are very

TABLE 2 Maxwell–Wagner–Sillars polarization of a volume comprising a set of elementary isotropic identical cells coupled together; influence of the volumetric content in polarizable cells for $\sigma_1 = 100 \text{ mS m}^{-1}$, $\sigma_2 = 10 \text{ mS m}^{-1}$ and $\varepsilon_2 = 10$.

Volumetric content in polarizable cells	Effective conductivity of the volume σ_e (mS m^{-1})	$\Delta\varepsilon_p$	τ (ns)
(a) $\varepsilon_1 = 10$			
0.05	15.3	11.0	2.4
0.10	21.0	12.0	2.7
0.15	27.1	13.0	3.1
0.20	33.8	14.1	3.4
(b) $\varepsilon_1 = 80$			
0.05	12.6	12.4	7.1
0.10	15.7	15.2	7.2
0.15	19.6	18.7	7.3
0.20	24.6	22.9	7.4
(c) $\varepsilon_1 = 800$			
0.05	13.0	15.9	57.5
0.10	16.8	23.9	54.0
0.15	21.8	35.7	48.4
0.20	28.2	55.0	42.0

TABLE 3 Maxwell–Wagner–Sillars polarization of a volume comprising a set of elementary isotropic identical cells coupled together; influence of the volumetric content in polarizable cells for $\sigma_1 = 10 \text{ mS m}^{-1}$, $\varepsilon_1 = 80$, $\sigma_2 = 1 \text{ mS m}^{-1}$ and $\varepsilon_2 = 10$.

Volumetric content in polarizable cells	Effective conductivity of the volume σ_e (mS m^{-1})	$\Delta\varepsilon_p$	τ (ns)
0.05	1.26	12.4	71.5
0.10	1.57	15.2	72.2
0.15	1.96	18.7	73.1
0.20	2.46	22.9	74.1

Note: Conductivities are divided by 10 compared to Table 2.

numerous, but the three cases, presented in Table 4, illustrate the influence of the cell properties, whereas the conductivity and the permittivity of the external medium remain fixed at $\sigma_2 = 10 \text{ mS m}^{-1}$ and $\varepsilon_2 = 10$ (as in Table 2), respectively, and the polarizable cells content remains at 10%. If σ_1 has either a fixed value at 50 mS m^{-1} or a logarithmic rate regular distribution of cell conductivity between 10 mS m^{-1} and 1000 mS m^{-1} , the effective conductivity stays around 15 mS m^{-1} , no far from the results in Table 2 (where $\sigma_1 = 100 \text{ mS m}^{-1}$ and the cell content equals 10%), whereas the effective permittivity strength, $\Delta\varepsilon_p$, and the time constant, τ , strongly vary with the cell permittivities. Moreover, the time constant easily overpasses 1 ns if the cell permittivity distribution comprises high values. However, high cell conductivity values counterbalance, resulting in a decrease of the time constant. In other words, for usual

TABLE 4 Maxwell–Wagner–Sillars polarization of a volume containing 10% of polarizable isotropic coupled cells inside an external medium of $\sigma_2 = 10 \text{ mS m}^{-1}$ and $\varepsilon_2 = 10$.

	Effective conductivity of the volume $\sigma_e \text{ (mS m}^{-1}\text{)}$	$\Delta\varepsilon_p$	$\tau \text{ (ns)}$
$\varepsilon_1 = 80$, $\sigma_1 \in [10, 1000 \text{ mS m}^{-1}]$	15.5	2.5	16
$\varepsilon_1 \in [10, 10,000]$, $\sigma_1 = 50 \text{ mS m}^{-1}$	15.0	70	550
$\varepsilon_1 \in [10, 10,000]$, $\sigma_1 \in [10, 1000 \text{ mS m}^{-1}]$	14.8	1.7	35

Note: The cells properties are non-identical with either constant values or uniform distributions.

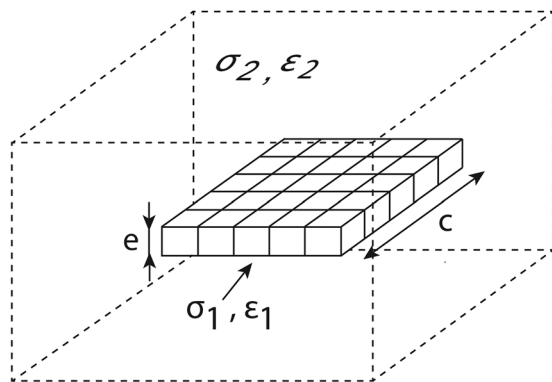


FIGURE 7 Platelet model corresponding to a series of adjacent small cubic cells with $\sigma_1 = 100 \text{ mS m}^{-1}$, $\varepsilon_1 = 80$, $\sigma_2 = 10 \text{ mS m}^{-1}$ and $\varepsilon_2 = 10$.

values of σ_1 , high values of ε_1 may generate high values of $\Delta\varepsilon_p$, which is intuitively expected, but also high values of the time constant, which is not intuitive. These conclusions confirm the results obtained for identical isotropic cells (this section) where an increase in ε_1 increases the time constants, whereas an increase in σ_1 reduces time constants.

Effective complex permittivity of platelet-like volume

This section addresses the effect of the shape of the polarized elementary volumes. This volume is a square flat platelet characterized by its flatness ratio c/e between its side c and its thickness e (Figure 7). In the MoM, it is broken down into a series of adjacent small cubic cells. Using the same values as previously, $\sigma_1 = 100 \text{ mS m}^{-1}$, $\varepsilon_1 = 80$, $\sigma_2 = 10 \text{ mS m}^{-1}$ and $\varepsilon_2 = 10$ (Table 3b), the variations with the flatness ratio are shown in Table 5.

In the direction perpendicular to the platelet, a Debye's type behaviour of the real part of the effective permittivity is observed with a time constant decreasing with the

flatness, whereas the effective conductivity is regularly increasing. In the direction parallel to the platelet, the time constant strongly increases with flatness, whereas the strength $\Delta\varepsilon_p$ remains very low in comparison to the perpendicular direction case; this impedes the time constant determination. In this case, the effective conductivity is slightly decreasing. The experimental work achieved by placing metallic particles inside wax by Sillars (1937) has already noted the high variability of the time constant with the shape and orientation of the particles. Dividing by a factor of 10 both conductivities, one gets the results shown in Table 5a,b. As expected, the effective conductivities are divided by 10, the strengths $\Delta\varepsilon_p$ do not significantly change and the time constants are increased by a factor of 10.

Having observed that the Maxwell–Wagner–Sillars polarization may explain a quite large distribution of relaxation parameters, one can consider molecular scale modelling.

Microscopic modelling of the relaxation of bound water molecules

Since the 1950s, many soil engineers and materials scientists have worked on the dielectric properties of the water layers adsorbed on clay particles (Goldsmith & Muir, 1960; Mamy, 1968; Muir, 1954; Nelson et al., 1969) for both kaolinite and smectite clays. They have established the importance of a 'Debye type' relaxation associated with the rotation of the adsorbed molecules and, at very low water contents, the dominant part of the first adsorbed layer (monolayer). However, when the water content increases, the respective parts of the successive layers of adsorbed water molecules and of the mobile hydrated cations are still in question (Calvet, 1975; Hall & Rose, 1978; Kaviratna et al., 1996; Vasilyeva et al., 2014).

Modelling the microscopic behaviour of bound molecules would be a very complex task, but one aspect can be tested here using the MoM, namely the possible impact of the external medium properties on the strength and the time constant of this particular relaxation. In this simplified approach, the magnitude of the unit molecular dipole moment can be considered identical to that of free molecules, but with a different time constant. Thus, one considers elementary volumes with a relative permittivity of 80 and with a distribution of time constants possibly varying with the molecule position in the coating layers and the nature of the solid mineral, for example a uniform distribution between $10 \mu\text{s}$ and $0.01 \mu\text{s}$. The objective is to study the impact of the surrounding medium properties, that is of the conductivity σ_2 and of the relative permittivity ε_2 , on the time constant distribution and the magnitude of the permittivity strengths.

TABLE 5 Maxwell–Wagner–Sillars polarization of platelet-like volume; evolution of the apparent relaxation parameters according to the flatness ratio.

Flatness ratio c/e	Effective conductivity σ_e //to the platelet (mS m ⁻¹)	Effective conductivity $\sigma_e \perp$ to the platelet (mS m ⁻¹)	Strength $\Delta\epsilon_p$ //to the platelet	τ (ns)//to the platelet	Strength $\Delta\epsilon_p \perp$ to the platelet	τ (ns) \perp to the platelet
(a) For $\sigma_1 = 100 \text{ mS m}^{-1}$, $\epsilon_1 = 80$, $\sigma_2 = 10 \text{ mS m}^{-1}$ and $\epsilon_2 = 10$						
11	2.30	0.55	0.47	5.0	94.3	1.62
21	2.02	1.03	3.79	3657	98.0	0.71
41	1.89	1.42	X	X	89.0	0.12
(b) For $\sigma_1 = 10 \text{ mS m}^{-1}$, $\epsilon_1 = 80$, $\sigma_2 = 1 \text{ mS m}^{-1}$ and $\epsilon_2 = 10$						
11	0.23	0.055	0.47	50.0	94.3	16.2
21	0.202	0.103	3.79	36,500	98.0	7.10
41	0.189	0.142	X	X	89.0	1.26

For this purpose, the MoM is again used to derive the effective relative permittivity corresponding to a random distribution of polarized cells inside an external volume of conductivity σ_2 and relative permittivity ϵ_2 . On this volume is applied a uniform primary electric field; the size of the volume is considered sufficiently small for the static approximation to be used. The cell complex permittivity is given by the Debye equation $\Delta\epsilon_p/(1+i\omega\tau)$ where $\Delta\epsilon_p = 80$.

For the time constant distribution, three different cases are considered. In the first, all the polarized cells have the same time constant $\tau = 1 \mu\text{s}$ (Figure 8a). In the second, τ may take two values $10 \mu\text{s}$ and 10 ns (Figure 8b). In the third, τ follows a uniform distribution between $10 \mu\text{s}$ and 10 ns (Figure 8c). In Figure 8, the surrounding medium has on the one hand $\sigma_2 = 100 \text{ mS m}^{-1}$ and $\epsilon_2 = 30$ (dashed lines), on the other, $\sigma_2 = 10 \text{ mS m}^{-1}$ and $\epsilon_2 = 10$ (continuous lines).

It is clear that the change in the external medium properties generates a shift in the absolute values of the real part of the effective relative permittivity, but neither $\Delta\epsilon_p$ nor τ (or its distribution) is modified. These criteria seem to be relevant for bound water molecules relaxation identification.

CONCLUSION AND PERSPECTIVES

The number of simulations presented above is limited and could be increased, but several paths can already be proposed. As seen in the theoretical examples by either properly modifying the geometrical shape of the polarized volumes or by changing their permittivity, conductivity or both, Maxwell–Wagner–Sillars effect can be invoked to fit any observed relaxation parameters. Consequently, this categorization is not discriminant (Jonscher, 1981). Moreover, as it is a ‘continuous medium approach’, it cannot inform about the underlying microscopic phenomena which are the final

objectives of any interpretation. Then, this denomination must be considered provisory, used while awaiting more complete information; it should not be placed at the same level as more meaningful denominations such as EDL polarization or semi-permeable membrane polarization. However, three common characteristics can be relevant to use such an ‘all scales’ modelling:

1. τ increases if the conductivities decrease and conversely (this intuitively corresponds to the situation where the more numerous the charges, the shorter the time constant (Abdulsamad et al., 2017, Bucker et al., 2019)) and the conductivity decrease of both the cells and the surrounding medium is evidenced by a decrease of the effective conductivity.
2. An increase in cell permittivity(ies) will significantly increase τ .
3. Depending on the orientation relative to platelet bodies, τ can vary on a very large range (especially when the direction parallel to platelet bodies is considered), far larger than the one observed for $\Delta\epsilon_p$.

The different examples illustrating the ‘General behaviour of complex permittivity in unsaturated surficial earth materials in the 100 Hz–10 MHz range’ section fit with the phenomenological formula presented in the ‘Phenomenological modelling of the complex permittivity’ section. All the observations are correctly modelled and thus can be described by a continuous distribution of relaxations (Jonscher universal behaviour) followed, for low saturation materials, by one marked relaxation (Cole–Cole behaviour) that adds to the high frequency permittivity corresponding to the water molecule rotations. It is possible to compare the three criteria defined before to some already-published data, for example those of Souffaché and Tabbagh (2021) where one relaxation and its evolution with the sample water content and electrical conductivity is clearly identified.

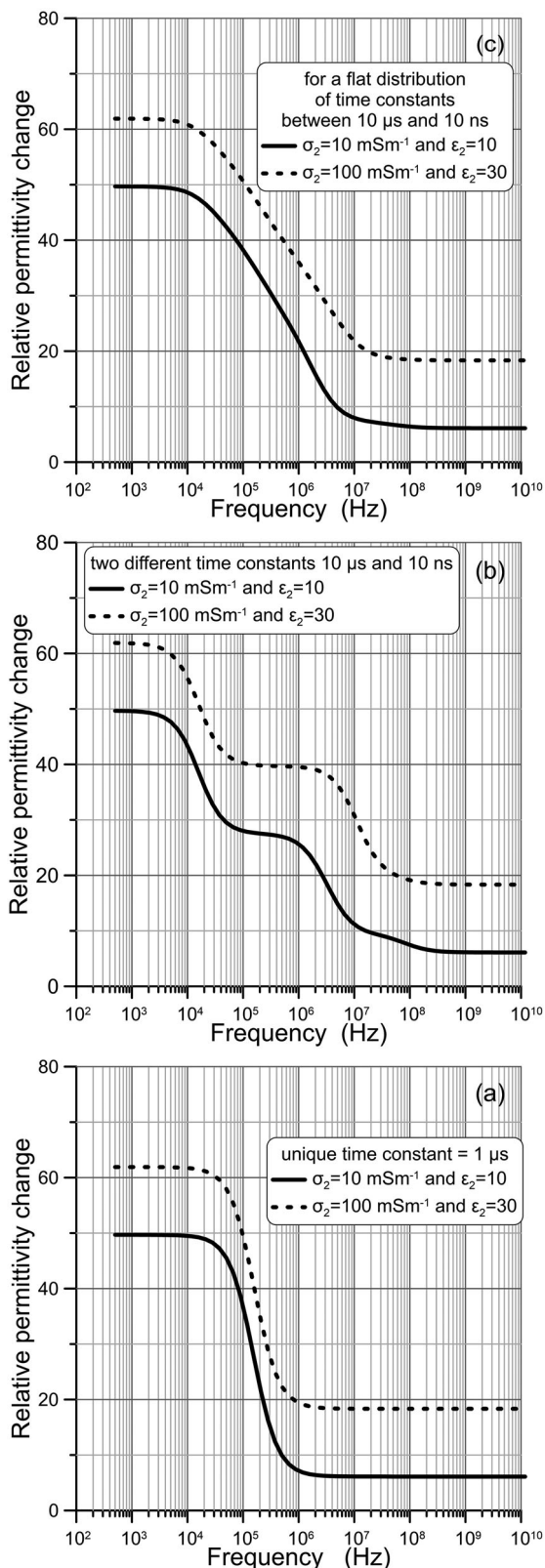


FIGURE 8 Frequency dependence of the real part of the effective relative permittivity for a random distribution of bound water polarizable cells (volumetric content 0.15) for $\sigma_2 = 10 \text{ mS m}^{-1}$ and $\varepsilon_2 = 10$ (solid lines) and for $\sigma_2 = 100 \text{ mS m}^{-1}$ and $\varepsilon_2 = 30$ (dashed lines): (a) for a unique time constant $\tau = 1 \mu\text{s}$, (b) for two different time constants $10 \mu\text{s}$ and 10 ns , (c) for a flat distribution of time constants between $10 \mu\text{s}$ and 10 ns .

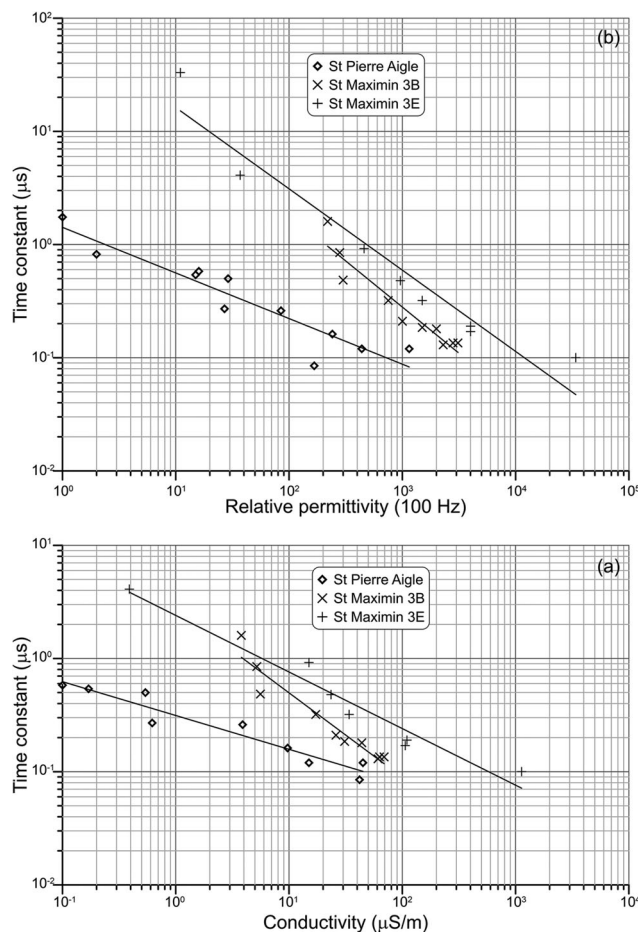


FIGURE 9 (a) Dependence of the time constant with the effective conductivity for three calcareous samples of progressing porosity (St Pierre Aigle 18.9%, St Maximin 3B 33% and St Maximin 3E 41%). (b) Dependence of the time constant with the effective relative permittivity for three calcareous samples of progressing porosity (St Pierre Aigle 18.9%, St Maximin 3B 33% and St Maximin 3E 41%).

Criterion (1) is illustrated in Figure 9a by drawing in Log–Log the dependence of the time constant on the effective conductivity where, if the dependence is linear, the curve would be parallel to the second bisector line (decrease in power minus one). For the lowest porosity (St Pierre Aigle, of 0.189 porosity), this is not the case; for St Maximin 3B, of 0.331 porosity, the dependence looks closer to the second bisector, but for the highest porosity (St Maximin 3E, of 0.41 porosity), the dependence of the time constant is reduced.

In the absence of information about the internal carriers of the electrical polarization, Figure 9 illustrates the dependence between the time constant and the effective permittivity (ε_j): The time constant decreases when the permittivity increases not far from a power law behaviour for the two highest porosities and the differences between the three samples are less marked than for the conductivity. This qualitative appreciation contraries criterion (2). Criterion (3) cannot be checked with this data set.

These three samples are a priori not representative of all soils and rocks present in the superficial layers, but it is clear that one cannot conclude that their behaviour agrees with the Maxwell–Wagner–Sillars modelling. It is thus of value to consider other models based on description at microscopic scale such as the resolution of the Poisson–Nernst–Planck equation.

As a first following step, we have considered the simple ‘bound water molecules’ model. As opposed to the Maxwell–Wagner–Sillars polarization, the relaxation parameters associated with the bound water molecules $\Delta\epsilon_p$ and τ are not dependent on the external medium properties, within the limits of the calculation errors. As these properties are always assessed, this criterion can be relevant and useful to identify and/or reject this phenomenon.

The regular logarithmic power frequency decrease of ϵ' at medium and high water contents (Figures 3 and 4) corresponds to the addition of a large distribution of time constants and will be considered in a holistic approach aiming to explore its relationship with the various parameters, at first the water content. The physical origin of the marked relaxation, observed for all unsaturated materials at lower water contents (Figure 4), between the regular logarithmic decrease and the high-frequency-independent limit, is not yet explained. It has been observed by other authors (Bobrov et al., 2022; Niu et al., 2020) for sandstones and suggests a possible semi-permeable membrane effect. This remains an important issue which will be the objective of future works in the (100 Hz–10 MHz) frequencies.











ACKNOWLEDGEMENTS

The work was achieved within the frame of the Métis Laboratory (UMR7619, Sorbonne University). The authors warmly thank all the participants of the geophysics team.

DATA AVAILABILITY STATEMENT

All the data used in the paper can be obtained freely by asking to the first author.

ORCID

A. Tabbagh  <https://orcid.org/0000-0001-7858-8359>
 B. Souffaché  <https://orcid.org/0000-0003-1607-8956>
 D. Jougnot  <https://orcid.org/0000-0003-4950-5766>
 A. Mainault  <https://orcid.org/0000-0002-9550-8055>
 F. Rejiba  <https://orcid.org/0000-0001-7557-5413>
 C. Schamper  <https://orcid.org/0000-0001-8276-5899>
 J. Thiesson  <https://orcid.org/0000-0001-7531-0474>
 C. Finco  <https://orcid.org/0000-0002-2085-3567>
 A. Mendieta  <https://orcid.org/0000-0002-8396-3237>
 F. Rembert  <https://orcid.org/0000-0003-3207-2466>
 R. Guérin  <https://orcid.org/0000-0001-7758-6984>

REFERENCES

- Abdulsamad, F., Florsch, N. & Camerlynck, C. (2017) Spectral induced polarization in a sandy medium containing semiconductor materials: experimental results and numerical modelling of the polarization mechanism. *Near Surface Geophysics*, 15(6), 669–682.
- Albrecht, R., Gourry, J.-C., Simonnot, M.-O. & Leyval, C. (2011) Complex conductivity response to microbial growth and biofilm formation on phenanthrene spiked medium. *Journal of Applied Geophysics*, 75, 558–564.
- Alvarez, R. (1973) Complex dielectric permittivity in rocks: a method for its measurement and analysis. *Geophysics*, 38(5), 920–940.
- Auken, E., Foged, N., Larsen, J.J., Lassen, K.V.T., Maurya, P.K., Moller-Dath, S., et al. (2019) tTEM—a towed transient electromagnetic system for detailed 3D imaging of the top 70 m of the subsurface. *Geophysics*, 84(1), E13–E22.
- Binley, A. & Slater, L. (2020) *Resistivity and induced polarization: theory and applications to the near-surface earth*. Cambridge: Cambridge University Press.
- Bobrov, P.P., Golikov, N.A., Kroshka, E.S. & Repin, A.V. (2022) Assessment of the permeability and pore size of quartz-based consolidated sedimentary rocks by dielectric spectroscopy in the frequency range of 1 kHz–500 MHz. *Journal of Applied Geophysics*, 204, 104750.
- Bröner, F. (2009) Complex conductivity measurements. In: Kirsch, R. (Ed.) *Groundwater geophysics—a tool for hydrogeology*. Berlin, Germany: Springer, pp. 119–153.
- Bücker, M., Flores Orozco, A., Undorf, S. & Kemna, A. (2019) On the role of Stern- and diffuse-layer polarization mechanisms in porous media. *Journal of Geophysical Research: Solid Earth*, 124(6), 5656–5677.
- Bücker, M. & Hördt, A. (2013) Analytical modelling of membrane polarization with explicit parameterization of pore radii and the electrical double layer. *Geophysical Journal International*, 194(2), 804–813.
- Calvet, R. (1975) Dielectric properties of montmorillonites saturated by bivalent cations. In: *Clay and clay minerals*, vol. 23. Berlin: Springer, pp. 257–265.
- Capello, M.A., Shaughnessy, A. & Caslin, E. (2021) The geophysical sustainability atlas: mapping geophysics to the UN Sustainable Development Goals. *The Leading Edge*, 40(1), 10–24.
- Cole, K.S. & Cole, R.H. (1941) Dispersion and absorption in dielectrics 1. Alternating current characteristics. *Journal of Chemical Physics*, 9, 341–351.
- Corwin, D.L. & Lesch, S.M. (2003) Application of soil electrical conductivity to precision agriculture: theory, principles, and guidelines. *Agronomy Journal*, 95(3), 455–471.
- Garrouch, A.A. & Sharma, M.M. (1994) The influence of clay content, salinity, stress, and wettability on the dielectric properties of brine-saturated rocks: 10 Hz to 10 MHz. *Geophysics*, 59(6), 909–917.
- Gebbers, R., Lück, E., Dabas, M. & Domsch, H. (2009) Comparison of instruments for geoelectrical soil mapping at the field scale. *Near Surface Geophysics*, 7(3), 179–190.
- Glaser, D.R. (2021) A site-specific comparison of permeability prediction models in alluvial sediments from physical and geoelectrical measurements. *Journal of Environmental and Engineering Geophysics*, 26(4), 315–322.
- Glaser, D.R., Barrowes, B.E., Shubitidze, F. & Slater, L.D. (2023) Laboratory investigation of high-frequency electromagnetic induction measurements for macro-scale relaxation signatures. *Geophysical Journal International*, 235(2), 1274–1291.
- Glaser, D.R., Shubitidze, F. & Barrowes, B.E. (2022) Standoff high-frequency electromagnetic induction response of unsaturated sands: a tank-scale feasibility study. *Journal of Environmental and Engineering Geophysics*, 27, 45–51.

- Goldsmith, B.J. & Muir, J. (1960) Surface ion effects in the dielectric properties of adsorbed water films. *Transactions of Faraday Society*, 56, 1656–1661.
- Gregory, A.P. & Clarke, R.N. (2005) Traceable measurements of the static permittivity of dielectric reference liquids over the temperature range 5–50°C. *Measurement Science and Technology*, 16, 1506–1516.
- Hall, P.G. & Rose, M.A. (1978) Dielectric properties of water adsorbed by kaolinite clays. *Journal of Chemical Society, Faraday Transactions 1*, 74, 1221–1233.
- Hermans, T., Goderniaux, P., Jougnot, D., Fleckenstein, J.H., Brunner, P., Nguyen, F. & Le Borgne, T. (2023) Advancing measurements and representations of subsurface heterogeneity and dynamic processes: towards 4D hydrogeology. *Hydrology and Earth System Sciences*, 27(1), 255–287.
- Howell, B.F. & Licastro, P.H. (1961) Dielectric behavior of rocks and minerals. *American Mineralogist*, 46, 269–288.
- Ishai, P.B., Talary, M.S., Caduff, A., Levy, E. & Feldman, Y. (2013) Electrode polarization in dielectric measurements: a review. *Measurement Science and Technology*, 24, 102001.
- Jonscher, A.K. (1977) The 'universal' dielectric response. *Nature*, 267, 673–679.
- Jonscher, A.K. (1981) Review. A new understanding of the dielectric relaxation of solids. *Journal of Material Science*, 16, 2037–2060.
- Kaviratna, P.D., Pinnavaia, T.J. & Schroeder, P.A. (1996) Dielectric properties of smectite clays. *Journal of Physical Chemistry of Solids*, 57(12), 1897–1906.
- Keller, G.V. & Licastro, P.H. (1959) Dielectric constant and electrical resistivity of natural-state cores. Geological Survey Bulletin 1052-H, 30 p.
- Kemna, A., Binley, A., Cassiani, G., Niederleithinger, E., Revil, A., Slater, L., et al. (2012) An overview of the spectral induced polarization method for near-surface applications. *Near Surface Geophysics*, 10, 453–468.
- Kessouri, P., Flageul, S., Vitale, Q., Buvat, S., Rejiba, F., Tabbagh, A. (2016) Medium-frequency electromagnetic device to measure electric conductivity and dielectric permittivity of soils. *Geophysics*, 81(1), E1–E16.
- Kessouri, P., Furman, A., Huisman, J.A., Martin, T., Mellage, A., Ntarlagiannis, D., et al. (2019) Induced polarization applied to biogeophysics: recent advances and future prospects. *Near Surface Geophysics*, 17(6), 595–621.
- Knight, R.M. & Nur, A. (1987) The dielectric constant of sandstones, 60 kHz to 4 MHz. *Geophysics*, 52(5), 644–654.
- Koch, K., Kemna, A., Irving, J. & Holliger, K. (2011) Impact of changes in grain size and pore space on the hydraulic conductivity and spectral induced polarization response of sand. *Hydrology and Earth System Sciences*, 15, 1785–1794.
- Kuras, O., Beamish, D., Meldrum, P.I. & Ogilvy, R.D. (2006) Fundamentals of capacitive resistivity technique. *Geophysics*, 71(3), G135–G152.
- Leroy, P. & Revil, A. (2009) A mechanistic model for the spectral induced polarization of clay minerals. *Journal of Geophysical Research*, 114, B10202.
- Lesmes, D.P. & Frye, K.M. (2001) Influence of pore fluid chemistry on the complex conductivity and induced polarization responses of Berea sandstone. *Journal of Geophysical Research*, 106(B3), 4079–4090.
- (de) Lima, O.A. L. & Sharma, M.M. (1992) A generalized Maxwell–Wagner theory for membrane polarization in shaly sands. *Geophysics*, 57(3), 431–440.
- Loewer, M., Günther, T., Igel, J., Martin, T., Kruschwitz, S. & Wagner, N. (2017) Ultra-broadband electrical spectroscopy of soils and sediments—a combined permittivity and conductivity model. *Geophysical Journal International*, 210, 1360–1373.
- Mamy, J. (1968) *Recherches sur l'hydratation de la montmorillonite: propriétés diélectriques et structure du film d'eau* [Thèse, Faculté des Sciences, Paris].
- Muir, J. (1954) Dielectric loss in water films adsorbed by some silicate clay minerals. *Transactions of Faraday Society*, 50, 249–254.
- Mullins, C.E. & Tite, M.S. (1973) Magnetic viscosity, quadrature susceptibility and frequency dependence of susceptibility in single-domain assemblies of magnetite and maghemite. *Journal of Geophysical Research*, 78(5), 804–809.
- Nelson, S.M., Huang, H.H. & Sutton, L.E. (1969) Dielectric study of water, ethanol and acetone adsorbed on Kaolinite. *Transactions of Faraday Society*, 65, 225–243.
- Niu, Q., Zhang, C. & Prasad, M., (2020). A framework for pore-scale simulation of effective electrical conductivity and permittivity of porous media in the frequency range from 1 mHz to 1 GHz. *Journal of Geophysical Research: Solid Earth*, 125(10), e2020JB020515.
- Nordsiek, S., Diamantopoulos, E., Hördt, A. & Durner, W. (2016). Relationships between soil hydraulic parameters and induced polarization spectra. *Near Surface Geophysics*, 14, 23–37.
- Ntarlagiannis, D. & Ferguson, A., (2009). SIP response of artificial biofilms. *Geophysics*, 74(1), A1–A5.
- Pellerin, L. (2002) Applications of electrical and electromagnetic methods for environmental and geotechnical investigations. *Survey of Geophysics*, 23(2), 101–132.
- Revil, A. (2013) Effective conductivity and permittivity of unsaturated porous materials in the frequency range 1 mHz–1 GHz. *Water Resource Research*, 49, 306–327.
- Revil, A., Binley, A., Mejus, L. & Kessouri, P. (2015) Predicting permeability from the characteristic relaxation time and intrinsic formation factor of complex conductivity spectra. *Water Resources Research*, 51, 6672–6700.
- Robinson, J., Slater, L., Weller, A., Keating, K., Robinson, T., Rose, C., et al. (2018) On permeability prediction from complex conductivity measurements using polarization magnitude and relaxation time. *Water Resources Research*, 54, 3436–3452.
- Samouëlian, A., Cousin, I., Tabbagh, A., Bruand, A. & Richard, G. (2005) Electrical resistivity survey in soil science: a review. *Soil & Tillage Research*, 83, 173–193.
- Schamper, C., Tabbagh, A., Flageul, S., Benech, C., Vitale, Q., Clément, B., et al. (2021) Electrostatic profiling and mapping of electrical resistivity and dielectric permittivity in an urban context—application to an archaeological site in Vienne (France). In: *27th European Meeting of Environmental and Engineering Geophysics, Bordeaux, France, Near Surface Geophysics conference, EAGE, August 28–September 1*.
- Scott, J.H., Carroll, R.D. & Cunningham, D.R. (1967) Dielectric constant and electrical conductivity measurements of moist rock: a new laboratory method. *Journal of Geophysical Research*, 72, 5105–5115.
- Sillars, R.W. (1937) The properties of a dielectric containing semiconducting particles of various shapes. *Journal of Institute of Electrical Engineering*, 80, 378–394.
- Simon, F.-X., Tabbagh, A., Donati, J.C. & Sarris, A. (2019) Permittivity mapping in the VLF-LF range using a multi-frequency EMI device: first tests in archaeological prospection. *Near Surface Geophysics*, 17(1), 27–41.
- Slater, L.D. & Glaser, D.R., (2003). Controls on induced polarization in sandy unconsolidated sediments and application to aquifer characterization. *Geophysics*, 68, 1542–1558.
- Smith-Rose, R.L. (1933) The electrical properties of soil for alternating currents at radio frequencies. *Proceedings of the Royal Society of London*, 140, 359–377.
- Souffaché, B., Kessouri, P., Blanc, P., Thiesson, J. & Tabbagh, A. (2016) First investigations of in situ electrical properties of limestone blocks of ancient monuments. *Archaeometry*, 58(5), 705–721.
- Souffaché, B. & Tabbagh, A. (2021) Laboratory study of the electrical properties of Lutetian limestones in the 100 Hz to 10 MHz frequency range. *Near Surface Geophysics*, 19(5), 573–582.
- Tabbagh, A., Hesse, A. & Grard, R. (1993) Determination of electrical properties of the ground at shallow depth with an

- electrostatic quadrupole: field trials on archaeological sites. *Geophysical Prospecting*, 41, 579–597.
- Tabbagh, A., Panissod, C., Guérin, R. & Cosenza, P. (2002) Numerical modelling of the role of water and clay content in soil and rock bulk electrical conductivity. *Journal of Geophysical Research*, 107(B11), 2318,.
- Tabbagh, A., Rejiba, F., Finco, C., Schamper, C., Souffaché, B., Camerlynck, C., Thiesson, J., Jougnot, D. & Maineult, A. (2021) The case for considering polarization in the interpretation of electrical and electromagnetic measurements in the 3 kHz to 3 MHz frequency range. *Surveys in Geophysics*, 42(2), 377–397.
- Topp, G.C., Davis, J.L. & Annan, A.P. (1980) Electromagnetic determination of soil water content: measurements in coaxial transmission lines. *Water Resources Research*, 16, 574–582.
- Vasilyeva, M.A., Gusev, Y.A., Shtyrlin, V.G., Greenbaum, A., Puzenko, A., Ben Ishai, P., et al. (2014) Dielectric relaxation of water in clay minerals. *Clays and Clay Minerals*, 62(1), 62–73.
- Viscarra Rossel, R.A. & Adamchuk, V.I. (2013) Proximal soil sensing. In: *Precision agriculture for sustainability and environmental protection*. Abington on Thames, UK: Routledge, Taylor & Francis Group.
- Woodward, W.H. H. (2021) *Broadband dielectric spectroscopy: a modern analytical technique* [Symposium Series]. Washington, DC: American Chemical Society.
- Wright, D.L., Smith, D.V., Abraham, J.D., Hutton, R.S., Bond, E.K., Cui, T.J., Alaeddin, A.A. & Chew, W.C. (2000) Imaging and modeling new VETEM data *Proceedings of SPIE*, 4084, 146–150

How to cite this article: Tabbagh, A., Souffaché, B., Jougnot, D., Maineult, A., Rejiba, F., Adler, P.M. et al. (2024) Experimental and numerical analysis of dielectric polarization effects in near-surface earth materials in the 100 Hz–10 MHz frequency range: First interpretation paths. *Near Surface Geophysics*, 1–14. <https://doi.org/10.1002/nsg.12302>